Electron states and microstructure of thin a-C:H layers

V. V. Afanas'ev and A. Stesmans

Department of Physics, University of Leuven, Celestijnenlaan 200D, B-3001 Leuven, Belgium

M. O. Andersson*

Department of Solid State Electronics, Chalmers University of Technology, S-41296 Gothenburg, Sweden

(Received 13 May 1996)

Thin layers of amorphous hydrogenated carbon (a-C:H) deposited on (100)Si/SiO$_2$ substrates were studied using atomic force microscopy, electron spin resonance (ESR), and internal photoemission spectroscopy. Layers with optical band gap in the range 3–0.7 eV were found to be homogeneous with respect to the interaction with oxygen under ultraviolet irradiation down to a lateral size of 5 Å. However, topographic features are developed under oxygen plasma exposure, where the decrease in the optical band gap is found to be correlated with the appearance of 300–500 Å lateral size features, ascribed to dense regions in a-C:H. Electron states near the Fermi level of a-C:H are related to electrically neutral diamagnetic network fragments. In the a-C:H of smallest band gap delocalized unpaired electrons are revealed, the observed ESR anisotropy suggesting a unidirectional ordering along the normal to the surface plain. Chainlike structures of carbon atoms are proposed as the network fragments responsible for the variation in the a-C:H optical gap width. [S0163-1829(96)04240-3]

I. INTRODUCTION

Amorphous hydrogenated carbon layers have unique electronic properties, propelling the efforts to trace the relation between the spectrum of electron states and microstructure. It is known that the optical band gap of amorphous hydrogenated carbon can be changed from almost zero to 4 eV just by varying the deposition conditions.[1] Yet the nature of the band-gap ruling network units is still unclear. An early model of Robertson and O'Reilly[2] provided a large impetus to the understanding of the electronic and optical properties of carbonaceous materials by introducing the idea of structural heterogeneity: The band-gap narrowing has been associated with the formation of clusters of six-fold aromatic rings, separated by regions with predominantly sp^3-bonded configurations of carbon atoms. According to this model, the typical optical band-gap values of 1–2 eV are related to the presence of clusters containing 10–40 planar rings. Such a degree of ordering, however, appeared unrealistic, particularly for the dense and mechanically hard layers of amorphous hydrogenated carbon (a-C:H) deposited under conditions of ion bombardment.[3]

Several theoretical works have recently addressed the nature of the band gap in dense a-C:H. The distortions of sp^2-bonded chains containing nonparallel sp^2 pairs[4] and dangling bonds[4,5] have been found to produce electron states near the Fermi level and narrow the band gap. Distortion of the six-fold ring from the planar configuration has been shown able to reduce the band gap down to 1.16 eV.[3] Even more significant narrowing may result from a pair of five- and seven-membered rings, down to 0.8 eV, if charge transfer between the rings is incorporated.[3] In the present work we will provide experimental evidence that the reduction of the optical band gap in thin layers of a-C:H from 3 to 0.7 eV is correlated with the presence of dense regions of 300–500 Å size. Inhomogeneity of a-C:H oxidation, however, is not observed down to a lateral size of 5 Å, suggesting the absence of large clusters with either pure sp^2 or sp^3 bonding. The unpaired electrons in narrow-gap a-C:H exhibit delocalization and anisotropic behavior, which suggests the presence of some degree of unidirectional ordering in the material. These observations support the hypothesis that the narrowing of the optical band gap in a-C:H is caused by sp^2 bonded chains of carbon atoms.

II. EXPERIMENT

The a-C:H samples were deposited by rf plasma decomposition of methane onto p-Si(100) wafers covered with 660 Å of thermally grown oxide. For the optical measurements witness samples were deposited onto transparent fused quartz substrates. The temperature of the substrate during deposition was maintained below 470 K. The thickness of the a-C:H layer was 400±50 Å, as determined by atomic force microscopy (AFM). By varying the bias of the substrate during a-C:H deposition, the properties of the layer can be changed. The deposition parameters of three types of the samples (labeled A, B, and C) are summarized in Table I. The optical band gap E_g of the deposited a-C:H layers was determined by extrapolating the $(\alpha h \nu)^{1/2}$-$h \nu$ plot down to $\alpha=0$, where α is the optical absorption coefficient of the film

TABLE I. Deposition parameters, optical band gap, and UV oxidation rate of a-C:H layers.

| Sample | Deposition parameters | | | Band gap (eV) | Oxidation rate (Å/min) |
	Pressure (mbar)	Bias (V)	Time (s)		
A	2	−198	48	3.0±0.05	10±1
B	1	−273	32	1.74±0.03	1.1±0.1
C	0.05	−900	60	0.70±0.02	0.8±0.1

and $h\nu$ is the photon energy;[6,7] E_g was found to vary from 0.7 to 3.0 eV.

It has been shown that structural variation in amorphous carbon influences the oxidation rate.[8] Moreover, it has been observed that during the annealing of sputtered carbon layers in air the difference in vaporization rate between regions of different structure results in development of topographic features,[9] which can be utilized for characterization of microstructure. The oxidation behavior of a-C:H layers may thus be expected to be sensitive to their deposition conditions. This is clearly seen from Table I, which shows the average oxidation rate of a-C:H layers by exposing them to air (1 atm) at 330 K under Xe discharge (resonant line $h\nu$ = 8.48 eV) ultraviolet (UV) radiation through a MgF$_2$ window with 0.1-mm air gap referred to as UV oxidation. The flux of UV photons beyond the window was about 1×10^{15} cm^{-2} s^{-1}. In order to verify the presence or absence of regions with different oxidation rate in the a-C:H layers the surface topography was analyzed before and after UV oxygen exposure using AFM operating in air.

The oxidation of a-C:H was also studied under conditions of rf oxygen plasma exposure [oxygen pressure $p(O_2)$=0.17 mbar, 0.86 1/h flow, 200 W] with the samples unbiased. In addition to the combined effect of UV radiation and atomic oxygen, attacking the a-C:H surface during UV oxidation, the oxygen ions present in the plasma can affect the oxidation rate through modifying the material by knock-on of carbon surface atoms and subplantation of oxygen. The comparison of the topographical features produced on a-C:H surfaces by UV oxidation and oxygen plasma treatment provides the possibility to reveal the effect of ion impact on the a-C:H structure.

The energy distribution of electron states in the a-C:H layers was analyzed using internal photoemission of electrons (IPE) from a-C:H into the thin SiO$_2$ layer covering the Si substrate. These experiments do not suffer from any modifications of the outer a-C:H layer possibly arising from ion bombardment during deposition and/or uncontrolled absorption of impurities from the ambient. By contrast, the band bending at the surface of a-C:H has been shown to cause problems in the evaluation of correlation energies for this material from the data of external photoemission spectroscopy.[10] In the case of IPE, however, electrons are optically excited within a-C:H and subsequently injected into SiO$_2$, thus producing a photocurrent. The physical processes involved in IPE are identical to those operational in external photoemission, except for the transport of electrons into an insulating layer.[11] Thus, the characterization of the energy distribution of electron states in an emitter can be done in essentially the same way as in the photoelectron yield spectroscopy.[10,12] In addition, thermally grown SiO$_2$ represents a high-quality insulator, able to sustain high electron fields during the IPE experiment. It is possible to trace the reduction of the interfacial barrier due to the Schottky effect and characterize the distribution of the electrostatic potential at the interface.[11] The latter is of particular interest, as the charged states are supposed to contribute to the density of states near the top of the a-C:H valence band.[3]

The samples for IPE experiments were prepared by forming a-C:H electrodes of 0.5×0.5 mm^2 size, with subsequent metallization by a 13.5-nm-thick gold layer, intended to provide a laterally uniform electric field over the sample area. Prior to IPE measurements, the structures were illuminated for 100 s by UV from a high-pressure Hg lamp in order to remove the holes trapped in the SiO$_2$ layer during deposition and processing of the a-C:H layers by neutralizing them by electrons injected from silicon.[13] Next, the Si/SiO$_2$/a-C:H/Au structures, with the gold electrode biased negatively, were illuminated by light from a 150-W Xe lamp dispersed with a monochromator (spectral resolution of 3 nm) and a cut-off filter. The relative light intensity was measured using a UV-sensitive Si photodiode either in combination with ($4<h\nu<6$ eV) or without ($2<h\nu<4$ eV) a sodium salycilate phosphor. The dc photocurrent through the oxide was measured using a Keithley 617 electrometer. The relative quantum yield of IPE was determined in terms of the photocurrent normalized to the incident light intensity. The strength of the electric field in the oxide (F) was calculated from the value of the bias applied between the silicon and gold, the oxide thickness, and the work function difference determined from the IPE current-voltage characteristics.[11]

To ensure that the IPE spectra are free from artifacts caused by plasma exposure of the oxide during a-C:H deposition, the IPE from gold into SiO$_2$ was studied in Si/SiO$_2$/Si structures prepared by evaporation of Au on the as-grown SiO$_2$ or subjected to a-C:H deposition followed by UV oxidation of the carbon overlayer. No difference in the spectral thresholds of IPE between these structures was found within an accuracy of 0.05 eV, indicating the absence of substantial changes in the energy of the edge of oxide conduction band with the respect to the Fermi level of gold. No contribution of the plasma-produced defects in SiO$_2$ to the photocurrent was observed. Noteworthy also is that the electrical breakdown measurements show no difference between Au and a-C:H covered SiO$_2$ layers: the breakdown electric field is in the range of 9–10 MV/cm in both cases. Thus the effect of plasma produced oxide defects on high-field injection and transport of electrons in the oxide layer is concluded to be insignificant.

The unpaired electron states in the a-C:H layers were characterized by electron spin resonance (ESR) spectroscopy at 4.3 K using a K-band spectrometer ($\sim$20.5 GHz). The system was operated in the derivative absorption mode under conditions of adiabatic slow passage.[14] The areal spin density was quantified by double numerical integration of the derivative absorption spectra. Absolute spin densities (in terms of $S=\frac{1}{2}$ centers assuming Curie susceptibility) were obtained using a calibrated Si:P intensity marker with g(4.3 K)=1.998 69$\pm$0.000 02. The absolute accuracy reached is estimated at $\approx$15%. ESR experiments were performed on nonmetallized a-C:H/SiO$_2$/Si structures.

III. RESULTS

A. AFM topography studies

The AFM images of the as-deposited a-C:H layers (not shown) are flat, characterized by a root mean square (rms) height deviation of 2–4 Å for a scan area of 2×2 μm^2; no distinct features are discernible. After removal of approximately 50% of the a-C:H layer by UV oxidation (determined by AFM step height measurements), the AFM images remain flat with similar rms values. The high-resolution images of the samples A, B, and C after the UV oxidation are shown in
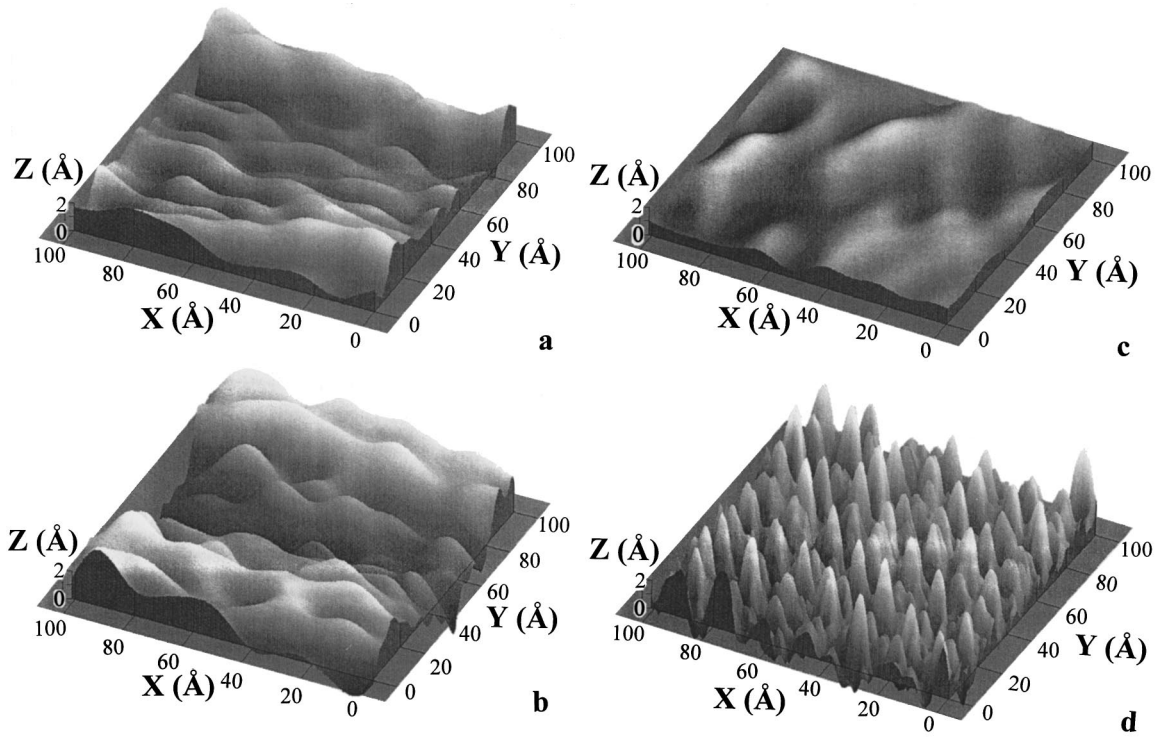
FIG. 1. High-resolution AFM images of the surface of samples (a) A, (b) B, and (c) C (see Table I) after UV oxidation. (d) The AFM image of a freshly cleaved mica surface is shown for comparison.

Figs. 1(a)–1(c), respectively. For comparison, the image of a cleaved mica sample is shown in Fig. 1(d), from which the lateral resolution of the AFM can be estimated to be better than 3 Å. Yet, no difference between samples $A-C$ can be distinguished, indicating the absence of regions with different oxidation rate down to a lateral size of approximately 5 Å.

The oxygen plasma oxidation of the a-C:H layers leads to substantial surface roughness, as evidenced by AFM images taken after 10-min plasma exposure [Figs. 2(a)–2(c)]. The etching time was restricted so as not to etch off the whole a-C:H layer. The surface of the wide-gap sample A shows the development of hill-like structures of 0.2–0.3 μm width and 50–70 Å height. Sample B shows the same type of structures superimposed with more narrow features of 300–500 Å lateral size and 40–60 Å height. The narrow-gap sample C shows both the small sharp features (similar to those observed on sample B) and deep (up to 200 Å peak-to-valley height) features of larger size. As the plasma exposure time increases, the features at the surface gradually smoothen and the separation between them increases, though they remain visible even after 50-min plasma oxidation. Taking into account the homogeneous character of oxygen interaction with a-C:H observed during UV oxidation, the development of the surface roughness during oxygen plasma oxidation likely relates to the action of the oxygen ions, bombarding the a-C:H surface.

The properties of the a-C:H layers are strongly affected by oxygen plasma exposure. First, all layers become mechanically soft as compared to the as-deposited state: they can be easily scratched by a steel needle. Second, the oxygen-plasma treated a-C:H layers can be easily dissolved in aqueous base solutions of NH_4OH (10%, 80 °C) or KOH

(20%, 60 °C), in contrast with the as-deposited or UV-oxidized layers. No difference is observed between the layers deposited under different conditions after 50-min plasma oxidation. It thus appears that oxygen ion bombardment induces substantial structural changes within a-C:H.

B. IPE spectroscopy of electron states

The quantum yield of IPE from a-C:H into SiO_2 as a function of photon energy is shown in Fig. 3 for the samples $A-C$ measured under equal bias ($F=4$ MV/cm). The cube root scale of the yield is chosen following the general description of the quantum yield spectral dependence for the case of photoemission from the valence band of a semiconductor.[15] The cubic increase of the electron photoemission yield into vacuum has been reported for a-C:H previously,[16] thus warranting this approximation. It is clearly seen that in the wide-gap sample A the spectral threshold of IPE is almost 1 eV higher than for the narrow-gap sample C. The yield curve of intermediate band-gap sample B appears to be a superposition of those of samples A and C. All spectral thresholds were found to be field dependent, suggesting significant Schottky reduction of the interfacial barrier.

At a certain photon energy above the thresholds, the yield starts to deviate from the third power behavior. The spectral position of this deviation (5.5–6 eV in sample A, 4.7 eV in sample B, and 4.5 eV in sample C) is independent of the applied bias. This is likely related to excitation of optical transitions within the a-C:H emitter.[11] The observed energies are close to the $\pi \rightarrow \pi^*$ transitions observed in optical spectra of wide-gap a-C:H [5.5,[16] 5.4, and 6.3 eV (Ref. 17)] and graphitelike material [4.9 (Ref. 18) and 4.8 eV (Ref. 16)]. A similar shift in $\pi \rightarrow \pi^*$ excitation energy between wide-gap
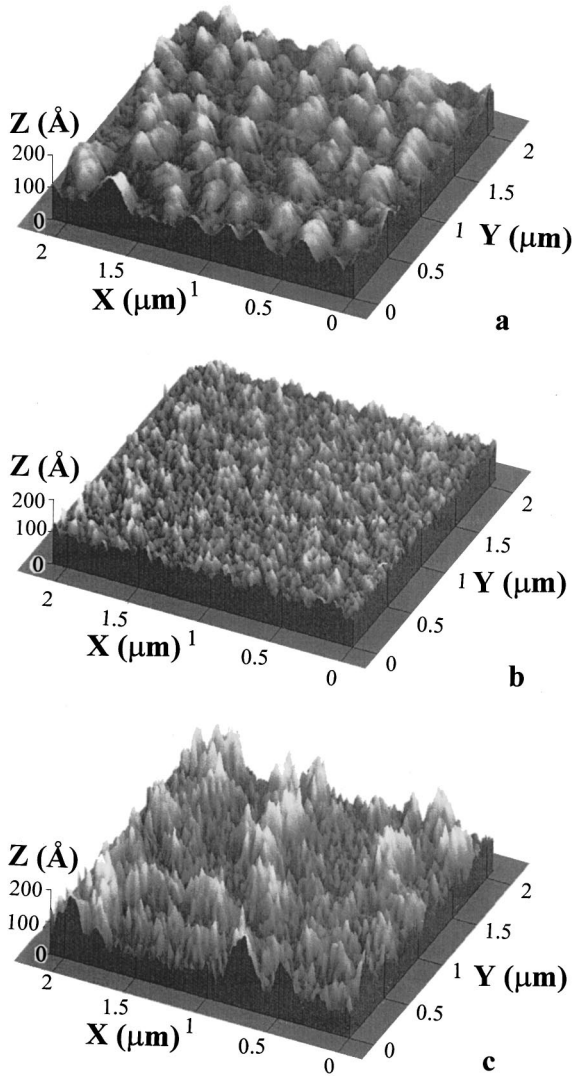
FIG. 3. IPE yield as a function of photon energy for the as-deposited samples A ($\bigcirc$), B ($\square$), and C ($\triangle$), measured at the strength of electric field in the oxide of 4 MV/cm. The electron transitions during IPE are schematically shown in the inset.

Moreover, the slope of the plot for as-deposited a-C:H layers is close to that for IPE from silicon up to the highest field (4 MV/cm) applied, suggesting a nearly ideal image force barrier. Only for the layers subjected to plasma oxidation is the slope reduced, likely because of oxide charging. The extrapolation of the spectral threshold field dependence to $F=0$ provides the true barrier height between the initial state of photoexcited electron and the bottom of the conduction band of SiO_2. It appears to be 4.6 eV for sample A and 3.6 eV for samples B and C. Taking into account the electron affinity of SiO_2 of 0.9 eV,[20] the latter value coincides with the Fermi level of graphite as determined by photoelectron spectroscopy (4.5 eV).[16]

C. ESR spectroscopy

In Figs. 6(a)–6(c) the ESR spectra are shown for each sample $(A-C)$ in the as-deposited state, after UV oxidation (1000-s exposure), and after plasma oxidation (50-min plasma exposure). Sample A shows a distinct signal at $g=2.0006$, with characteristic powder pattern. This signal, corresponding to a density of about 1×10^{13} cm^{-2}, originates from dangling Si bonds in the SiO_2 layer (E'_γ center).[21] The

FIG. 2. Wide scan AFM images of the surface of samples (a) A, (b) B, and (c) C after 10-min plasma oxidation.

a-C:H and graphite (from 6.5 to 4.5 eV) has been observed in the electron-energy-loss spectra.[19] On this basis we ascribe the observed reduction in the IPE yield with the upcoming $\pi \rightarrow \pi^*$ transitions in a-C:H.

The UV oxidation was found to have little effect on the IPE characteristics. In contrast, the oxygen plasma exposure modified the IPE spectral curve drastically. Figure 4 shows the IPE yield of the wide-gap sample A subjected to 50-min plasma oxidation for various electric-field strengths in the oxide. The spectrum resembles that of the as-deposited narrow-gap sample C (Fig. 3) in terms of the yield value, the IPE spectral threshold, and the $\pi \rightarrow \pi^*$ transition feature. Similar spectral distributions of the IPE yield were observed after plasma oxidation of samples B and C, suggesting conversion by plasma oxidation of all the layers to a carbon phase close to narrow-gap carbon.

The IPE spectral thresholds of a-C:H layers are plotted in Fig. 5 as a function of the square root of electric field in the oxide, together with the IPE from a Si(100) surface into SiO_2. The ideal image force potential barrier should exhibit linear reduction[15] of the barrier height versus $\sqrt{F}$. It is seen that this dependence is observed in all the cases indeed.
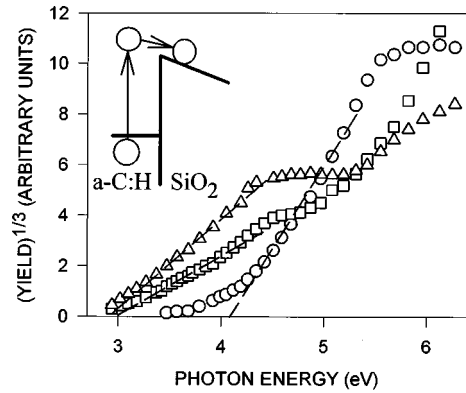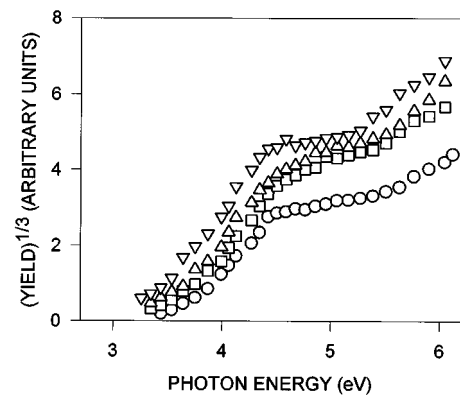

FIG. 4. IPE yield as a function of photon energy for sample A subjected to 50-min plasma oxidation, measured at electric field strengths in the oxide of 0.5 ($\bigcirc$), 1.0 ($\square$), 2.0 ($\triangle$), and 3.0 ($\triangledown$) MV/cm.
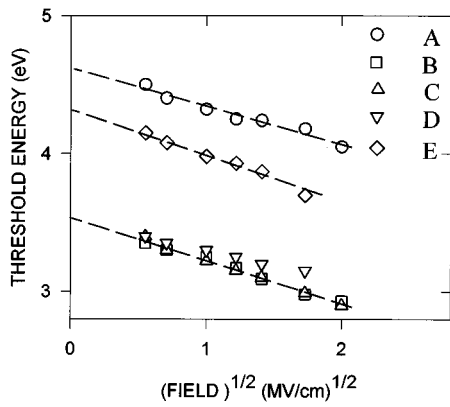
FIG. 5. Spectral thresholds of IPE as a function of the square root of the applied electric field in the as-deposited samples A, B, C, and sample A subjected to 50-min plasma oxidation (D). The thresholds of IPE from Si(100) into SiO$_2$ measured on a Si/SiO$_2$/Au structure are shown for comparison (E).

generation of large amounts of these centers in an electrically neutral state during illumination of SiO$_2$ by 10-eV photons through a semitransparent Al electrode has been recently reported.[22] The latter conditions are close to those encountered during plasma-assisted deposition of a-C:H in the present experiments; the appearance of E'_γ centers is thus not surprising. The only observed signal belonging to a-C:H is a broad isotropic line at $g = 2.0031 \pm 0.0002$. Signals with close g values were reported earlier in various a-C:H layers.[7,23–27] This signal slightly increases after UV oxidation. After plasma oxidation the E'_γ center becomes invisible by ESR, apparently due to passivation of the dangling bonds by hydrogen released from the a-C:H layer, also the $g = 2.0031$ appears to have disappeared; only a weak $g = 2.0055$ line remains.

The ESR spectrum [Fig. 6(b)] of the as-deposited sample B shows an intense, isotropic broad line with $g = 2.0019$, corresponding to 1.5×10^{15} spins/cm^2, superposed by a second signal. After UV exposure the main line is substantially reduced and the second characteristic two-peak signal can now be recognized as the E'_γ center ($g = 2.0006$). Clearly, plasma oxidation (curve 3) eliminates both signals.

The as-deposited sample C shows only one intense signal [Fig. 6(c), curve 1] of $\approx 2 \times 10^{15}$ spins/cm^2, barely affected by UV exposure (curve 2). This narrow line (peak-to-peak width $\Delta B_{pp} = 2.23$ G at 4.3 K) shows anisotropy with respect to the orientation of the applied magnetic field $\mathbf{B}$; at 4.3 K, $g_\parallel = 2.001\,83 \pm 0.000\,04$ and $g_\perp = 2.0029 \pm 0.000\,04$ for $\mathbf{B}$ parallel and perpendicular to the main sample surface, respectively. As the temperature increases, the anisotropy collapses, resulting in an isotropic behavior above ≈ 30 K. It is interesting to note that a single narrow line spectrum was reported in a-C:H at higher temperature ($T > 77$ K).[27,28] The absence of a powder pattern and dipole broadening suggests that this signal stems from delocalized electrons among several accessible sites, while the anisotropy suggests preferential alignment of these sites along one direction. This situation can be compared to that for graphite, where a strong anisotropy is found at 77 K ($g_\parallel = 2.127$ and $g_\parallel = 2.0026$).[29] However, the anisotropy observed here is much weaker than found in graphite. It seems unlikely that the present ESR

signal is due to graphite inclusions in a-C:H. Plasma oxidation removes the anisotropic signal (curve 3); only a weak line remains at $g = 2.0055$, like in sample A.

IV. DISCUSSION

The experimental results demonstrate that variation of the deposition conditions of a-C:H layers induces changes not only in the optical band-gap width and energy distribution of electron states, but also in the medium-range microstructure (10–100 Å range) and type of ESR active states. Moreover, all these properties appear to be sensitive to an oxygen plasma exposure. Based on these findings, we will try in this section to infer some correlation between the structure and electronic properties of a-C:H. It is recognized that the present results may not be general, but merely reflecting the properties of only a particular type of densified a-C:H layers produced by plasma-assisted decomposition of methane. Nevertheless, the conclusions about the nature of electron states in our layers may be of interest for other carbonaceous materials, as the common nature of the band gap, originating from sp^2-bonded fragments, has been evidenced by numerous theoretical investigations.[1–5]

The development of surface asperity under oxygen plasma exposure, in contrast to UV oxidation, points to the importance of the impact effect of oxygen ions as a primary source of lateral nonuniformity. We suggest the lateral fluctuations in the a-C:H layer density to be responsible for the observed development of the surface asperity. The projected range of the primary oxygen ions will decrease as the local density increases, so dense regions will screen underlying a-C:H layers. Moreover, secondary carbon ions, knocked off from the surface layers of a-C:H, will efficiently be stopped inside the dense regions thus adding to their size, in balance with the sputtering action of primary ions. The low-density regions, by contrast, allow deep implantation of oxygen, thus increasing the effective layer volume available for oxidation. The result is an enhanced oxidation of less dense regions in the plasma, leading to a ''porous'' surface. The development of a porous surface was recently observed during low-temperature oxidation of carbon layers prepared by sputtering of graphite in Ar plasma onto Si substrates;[10] after thermal oxidation the surface of amorphous carbon consists of graphitelike regions 300–500 Å across. As mentioned, features of the same size are observed here after plasma etching of samples B and C (Fig. 2) and the IPE spectrum after the plasma oxidation (Fig. 4) resembles that of the graphitelike material (Fig. 3). After prolonged plasma oxidation only the densified carbon phase seems to remain. Within the framework of the density fluctuational model, the main structural difference in the as-deposited state between the wide-gap sample A and narrow-gap samples B and C is the presence of densified regions in the latter. Note that all three samples show a laterally uniform oxidation in the absence of ion bombardment. Taking into account the difference in the rate of oxidation by atomic O by factor of 30–50 between sp^2-(graphite) and sp^3-bonded (diamond) carbon,[8] the uniform oxidation suggests laterally homogeneous distribution of sp^2- and sp^3-bonded fragments. Two factors may be responsible for the local variations of the a-C:H density: one, the variation of hydrogen content, as suggested by nuclear mag-
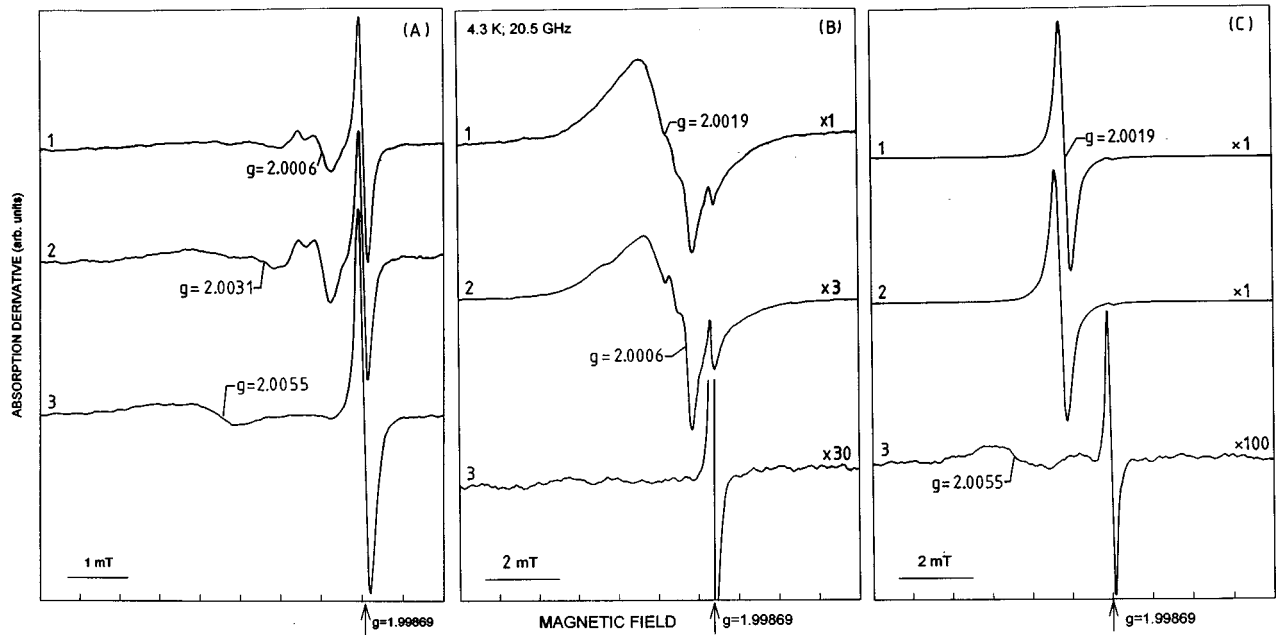
FIG. 6. K-band ($\sim$20.5 GHz) ESR spectra ($T=4.3$ K) of samples (a) A, (b) B, and (c) C. Shown for each sample type is the spectrum observed in the as-deposited state (1), after 1000-s UV oxidation (2), and after 50-min plasma oxidation (3). The spectra are taken at a microwave power $\leq$30 nW to avoid saturation effects. The signal at $g=1.99869$ stems from a Si:P marker.

netic resonance studies,[30] and the other, the changes in the network topology, which, in turn, may also affect the behavior of hydrogen.[31] In both cases, the compact microstructure is believed to provide the highest resistance against oxidation.[8]

The presence of the dense regions in the as-deposited samples B and C and in all three samples after the plasma oxidation correlates with the development of electron states near the Fermi level of graphite and with the shift of the $\pi\rightarrow\pi^*$ transition from 5.5 to 4.5 eV, the value characteristic for graphite. This allows us to call this distribution of electron states the graphitelike one. However, ESR spectroscopy clearly shows either large differences in the unpaired electron states [compare samples A and B, Figs. 6(a) and 6(b)], or the near absence of the ESR active states after plasma oxidation [Figs. 6(a)–6(c)]. It thus appears that the graphitelike electron spectrum is not always associated with the graphitelike structure, known to produce a distinctly anisotropic ESR signal.[29] The densities of the unpaired electrons in the as-deposited samples B and C do not differ more than 30%, but the density of the graphitelike states in sample B is approximately one order of magnitude lower than in sample C, as observed by IPE (cf., Fig. 3, note the cube root yield scale). Consequently, we cannot correlate the density of states near the Fermi level with the presence of unpaired electrons.

The field dependences of the spectral threshold of the IPE from the states near the top valence states of a-C:H into SiO_2 obey the ideal image force model. It means that there are no electric fields, such as, charged centers in a-C:H, perturbing the image force potential. Within the accuracy of the IPE data we can estimate the strength of the perturbing field not to exceed 0.3 MV/cm. It means that there are no uncompensated charges within a distance of 3–4 nm from the point of electron emission, i.e., the mean distance between charged defects is larger than 6–8 nm. Using this estimate, the vol-

ume concentration of uncompensated charge is calculated to be less than 5×10^{18} cm^{-3}. This amount is insufficient to account for the states near Fermi level and the unpaired electrons, for which a volume concentration of $(3–5)\times10^{20}$ cm^{-3} is obtained in samples B and C if assuming uniform distribution of unpaired spins over the 400-Å-thick layer. This indicates that the electron states near the Fermi level originate from neutral network fragments in dense regions of a-C:H and are related to paired electron states.

Support for the above hypothesis can be inferred from the ESR data of narrow-gap a-C:H samples. The anisotropy of the ESR signal observed in sample C ($g_\parallel<g_\perp$) is inverted with respect to graphite ($g_\parallel>g_\perp$).[29] If the same type of electron states (electrons delocalized in sp^2-bonded fragments) are responsible for both signals, the inversion of anisotropy can be explained by changes in the spatial orientation of these fragments with respect to the sample surface, i.e., the equivalent states in a-C:H have some degree of alignment along the normal to the sample surface. As the temperature increases, the anisotropy is motionally averaged out, which indicates the presence of equivalent states in the direction parallel to the surface, yet less favorable energetically. This behavior suggests a chain structure similar to the one proposed recently by Walters and Newport,[32] with some unidirectional ordering along the normal to the surface plane (columnar structure).

The correlation between the density of ESR active centers and the conductivity of a-C:H has been reported earlier,[28] indicating that the electron states near the Fermi level of a-C:H can be responsible for the presence of unpaired electrons. Our results are in line with these observations: strong ESR signals are observed only in the samples showing a well-developed graphitelike spectrum of electron states (cf., Figs. 3, 4, and 6). However, some degree of order has to be present in the layer to allow free motion of an unpaired elec-

tron between equivalent states. When the density of states near the Fermi level is low, like in sample B, the g value of the ESR line remains the same as in sample C (high density of states), but the signal broadens, suggesting nonequivalency of electron states. The broadening has been shown to be associated with the presence of hydrogen,[28] and C-H bonds can be considered as a factor that reduces the number of available equivalent sites for an electron. In the wide-band-gap sample A the ESR signal from delocalized electrons disappears and only the signal with $g = 2.003$ is left, ascribed to isolated carbon dangling bonds.[25,26,33] We hypothesize that delocalization of electrons occurs among the states near the Fermi level of graphitelike a-C:H. Some percentage of the corresponding network fragments, e.g., chains, may contain an odd number of electrons thus being ESR active.

From the correlations between width of the optical gap of the a-C:H and the properties studied in the present work, we propose that graphitelike electron states may be related with densified regions of a-C:H. These fragments contain chain elements and have a low concentration of bonded hydrogen. This inference, of course, requires further affirmation.

V. CONCLUSION

The optical band-gap narrowing in thin a-C:H layers produced by plasma-assisted deposition is found to be correlated with the presence of densified regions in the a-C:H layer, not, however, with the formation of regions of different chemical carbon configuration. The electron states near the Fermi level were found to be paired and related to electrically neutral network fragments. In the narrow-gap layers, delocalization of electrons is observed, but not corresponding to a graphitelike configuration; the anisotropy of the observed ESR signal suggests unidirectional ordering in narrow-gap a-C:H layers along the normal to the surface plane. Chainlike structures of sp^2-bonded carbon atoms are hypothesized as the network elements responsible for a-C:H optical gap narrowing.

ACKNOWLEDGMENTS

*Present address: Volvo Car Corporation, S-4058, Gothenburg, Sweden.

[1] J. Robertson, Adv. Phys. **35**, 317 (1986).

[2] J. Robertson and E. P. O'Reilly, Phys. Rev. B **35**, 2946 (1987).

[3] J. Robertson, Diamond Relat. Mater. **4**, 297 (1995).

[4] C. H. Lee, W. R. L. Lambrecht, B. Segall, P. C. Kelires, Th. Frauenheim, and U. Stephan, Phys. Rev. B **49**, 11 448 (1994).

[5] U. Stephan, Th. Frauenheim, P. Blaudeck, and G. Jungnickel, Phys. Rev. B **49**, 1489 (1994); S. Uhlmann, Th. Frauenheim, and U. Stephan, *ibid.* **51**, 4541 (1995).

[6] J. Tauc, R. Grigirovici, and A. Vancu, Phys. Status Solidi **15**, 627 (1996).

[7] D. Dasgupta, F. Demichelis, C. F. Pirri, and A. Tagliaferro, Phys. Rev. B **43**, 2131 (1991).

[8] E. B. D. Bourdon, A. Raveh, S. C. Gujrathi, and L. Martinu, J. Vac. Sci. Technol. A **11**, 2530 (1993).

[9] J. M. Yanez-Limon, F. Ruiz, J. Gonzalez-Hernandez, B. S. Chao, and S. R. Ovshinsky, J. Appl. Phys. **78**, 3015 (1995).

[10] J. Ristein, J. Schäfer, and L. Ley, Diamond Relat. Mater. **4**, 508 (1995).

[11] V. K. Adamchuk and V. V. Afanas'ev, Prog. Surf. Sci. **41**, 109 (1992).

[12] K. Winer and L. Ley, Phys. Rev. B **36**, 6072 (1987).

[13] J. M. M. de Nijs, K. G. Druijf, V. V. Afanas'ev, E. van der Drift, and P. Balk, Appl. Phys. Lett. **65**, 2428 (1994).

[14] G. Van Gorp and A. Stesmans, Phys. Rev. B **45**, 4244 (1992).

[15] C. N. Berglund and R. J. Powell, J. Appl. Phys. **42**, 573 (1971).

[16] M. De Seta, P. Fiorini, F. Coppola, and F. Evangelisti, J. Non-Cryst. Solids **137/138**, 867 (1991).

[17] M. Nakayama, M. Shibahara, K. Maruyama, and K. Kamata, J. Mater. Sci. Lett. **12**, 1380 (1993).

[18] E. A. Taft and H. R. Philipp, Phys. Rev. **138**, A197 (1965).

[19] J. Fink, Th. Muller-Heinzerling, J. Pfluger, B. Schreerer, B. Dischler, P. Koidl, A. Bubenzer, and R. E. Sah, Phys. Rev. B **30**, 4713 (1984).

[20] S. M. Sze, *Physics of Semiconductor Devices,* 2nd ed. (Wiley, New York, 1981), p. 397.

[21] D. L. Griscom, Nucl. Instrum. Methods B **1**, 481 (1984).

[22] V. V. Afanas'ev, J. M. M. de Nijs, P. Balk, and A. Stesmans, J. Appl. Phys. **78**, 6481 (1995).

[23] D. J. Miller and D. R. McKenzie, Thin Solid Films **108**, 257 (1983).

[24] I. Watanabe and T. Okumura, Jpn. J. Appl. Phys. **24**, C122 (1985).

[25] S. P. Wong, S. Peng, N. Ke, and P. Li, Nucl. Instrum. Methods B **80/81**, 1494 (1993).

[26] Y. Bounouh, L. Chaded, A. Sadki, M. L. Theye, C. Cardinaud, M. Zarrabian, J. von Bardeleben, K. Zellama, J. Cernogora, and J.-L. Fave, Diamond Relat. Mater. **4**, 492 (1995).

[27] M. Fanciulli and T. D. Moustakas, Diamond Relat. Mater. **1**, 773 (1992).

[28] M. Hoinkis, E. D. Tober, R. L. White, and M. S. Crowder, Appl. Phys. Lett. **61**, 2653 (1992).

[29] G. Wagoner, Phys. Rev. **118**, 647 (1960).

[30] C. Jager, J. J. Titman, and R. J. Newport, Thin Solid Films **227**, 3 (1993); C. Jager, J. Gottwald, H. W. Spiess, and R. J. Newport, Phys. Rev. B **50**, 846 (1994).

[31] Y. Bounouh, M. L. Theye, A. Dehbi-Alaoui, A. Matthews, and J. P. Stoquert, Phys. Rev. B **51**, 9597 (1995).

[32] J. K. Walters and R. J. Newport, J. Phys.: Condens. Matter **7**, 1755 (1995).

[33] Y. Mori, Y. Show, M. Deguchi, H. Yagi, H. Yagyu, N. Eimori, T. Okada, A. Hatta, K. Nishimura, M. Kitabatake, T. Ito, T. Hiaro, T. Izumi, T. Sasaki, and A. Hiraki, Jpn. J. Appl. Phys. **32**, L987 (1993).